Mathematical Biosciences and Engineering

http://www.aimspress.com/journal/MBE

MBE, 18(4): 4834–4859.
DOI: 10.3934/mbe.2021246
Received: 24 December 2020
Accepted: 31 May 2021
Published: 03 June 2021

Research article

Cancer detection through Electrical Impedance Tomography and optimal control theory: theoretical and computational analysis

Ugur G. Abdulla*, Vladislav Bukshtynov and Saleheh Seif

Department of Mathematical Sciences, Florida Institute of Technology, Melbourne, FL 32901, USA

* **Correspondence:** Email: abdulla@fit.edu.

Abstract: The Inverse Electrical Impedance Tomography (EIT) problem on recovering electrical conductivity tensor and potential in the body based on the measurement of the boundary voltages on the m electrodes for a given electrode current is analyzed. A PDE constrained optimal control framework in Besov space is developed, where the electrical conductivity tensor and boundary voltages are control parameters, and the cost functional is the norm difference of the boundary electrode current from the given current pattern and boundary electrode voltages from the measurements. The novelty of the control-theoretic model is its adaptation to the clinical situation when additional "voltage-to-current" measurements can increase the size of the input data from m up to $m!$ while keeping the size of the unknown parameters fixed. The existence of the optimal control and Fréchet differentiability in the Besov space along with optimality condition is proved. Numerical analysis of the simulated model example in the 2D case demonstrates that by increasing the number of input boundary electrode currents from m to m^2 through additional "voltage-to-current" measurements the resolution of the electrical conductivity of the body identified via gradient method in Besov space framework is significantly improved.

Keywords: cancer detection; Electrical Impedance Tomography; PDE constrained optimal control; Fréchet differentiability; projective gradient method

1. Introduction and problem description

This paper analyzes inverse EIT problem of estimating an unknown conductivity inside the body based on voltage measurements on the surface of the body when electric currents are applied through a set of contact electrodes. Let $Q \in \mathbb{R}^n$ be an open and bounded set representing body, and assume $A(x) = \left(a_{ij}(x)\right)_{ij=1}^{n}$ be a matrix representing the electrical conductivity tensor at the point $x \in Q$. Electrodes, $(E_l)_{l=1}^{m}$, with contact impedances vector $Z := (Z_l)_{l=1}^{m} \in \mathbb{R}_+^m$ are attached to the periphery of the body, ∂Q. Electric current vector $I := (I_l)_{l=1}^{m} \in \mathbb{R}^m$ is applied to the electrodes. Vector I is called *current*

pattern if it satisfies conservation of charge condition

$$\sum_{l=1}^{m} I_l = 0. \tag{1.1}$$

The induced constant voltage on electrodes is denoted by $U := (U_l)_{l=1}^m \in \mathbb{R}^m$. By specifying ground or zero potential it is assumed that

$$\sum_{l=1}^{m} U_l = 0. \tag{1.2}$$

EIT problem is to find the electrostatic potential $u : Q \to \mathbb{R}$ and boundary voltages U on $(E_l)_{l=1}^m$. The mathematical model of the EIT problem is described through the following boundary value problem for the second order elliptic partial differential equation:

$$-\sum_{i,j=1}^{n} \left(a_{ij}(x)u_{x_j}\right)_{x_i} = 0, \qquad x \in Q \tag{1.3}$$

$$\frac{\partial u(x)}{\partial \mathcal{N}} = 0, \qquad x \in \partial Q - \bigcup_{l=1}^{m} E_l \tag{1.4}$$

$$u(x) + Z_l \frac{\partial u(x)}{\partial \mathcal{N}} = U_l, \qquad x \in E_l,\ l = \overline{1,m} \tag{1.5}$$

$$\int_{E_l} \frac{\partial u(x)}{\partial \mathcal{N}} ds = I_l, \qquad l = \overline{1,m} \tag{1.6}$$

where

$$\frac{\partial u(x)}{\partial \mathcal{N}} = \sum_{i,j} a_{ij}(x) u_{x_j} \nu^i$$

be a co-normal derivative at x, and $\nu = (\nu^1, ..., \nu^n)$ is the outward normal at a point x to ∂Q. Electrical conductivity matrix $A = (a_{ij})$ is positive definite with

$$\sum_{i,j=1}^{n} a_{ij}(x)\xi_i\xi_j \geq \mu \sum_{i=1}^{n} \xi_i^2,\ \forall \xi \in \mathbb{R}^n; \quad \mu > 0. \tag{1.7}$$

The following is the

EIT Problem: *Given electrical conductivity tensor A, electrode contact impedance vector Z, and electrode current pattern I it is required to find electrostatic potential u and electrode voltages U satisfying* (1.2)–(1.6):

$$(A, Z, I) \longrightarrow (u, U).$$

The goal of the paper is to analyze the inverse EIT problem of determining conductivity tensor A from the measurements of the boundary voltages U^*.

Inverse EIT Problem: *Given electrode contact impedance vector Z, electrode current pattern I and boundary electrode measurement U^*, it is required to find electrostatic potential u and electrical conductivity tensor A satisfying* (1.2)–(1.6) with $U = U^*$.

EIT problem has many important applications in medicine, industry, geophysics and material science [1]. Mathematical model (1.2)–(1.6) for the EIT Problem, referred as complete electrode model, was suggested in [2] in the isotropic case $A = \sigma I$, where I is a unit matrix (Eq (1.8)). This model suggests the replacement of the complete potential measurements along the boundary with measurements of constant potential along the electrodes with contact impedances. In [2] it was demonstrated that the complete electrode model is physically more relevant, and it is capable of predicting the experimentally measured voltages to within 0.1 percent. Existence and uniqueness of the solution to the problem (1.2)–(1.6) was proved in [2].

We are especially motivated by medical applications on the detection of cancerous tumors from breast tissue or other parts of the body. Relevance of the inverse EIT problem for cancer detection is based on the fact that the conductivity of the cancerous tumor is higher than the conductivity of normal tissues [3]. Inverse EIT Problem is an ill-posed problem and belongs to the class of so-called Calderon type inverse problems, due to celebrated work [4], where the well-posedness of the inverse problem for the identification of the conductivity coefficient $\sigma : \Omega \to \mathbb{R}$ of the second-order elliptic PDE

$$div(\sigma(x)\nabla u) = 0 \tag{1.8}$$

through Dirichlet-to-Neumann or Neumann-to-Dirichlet boundary maps is presented. Significant development in Calderon's inverse problem in the class of smooth conductivity functions with spatial dimension $n \geq 3$, concerning questions on uniqueness, stability, reconstruction procedure, reconstruction with partial data was achieved in [5–10]. Global uniqueness in spatial dimension $n = 2$ and reconstruction procedure through scattering transform and employment of the D-bar method was presented in a key paper [11]. Further essential development of the D-bar method for the reconstruction of discontinuous parameters, regularization due to the inaccuracy of measurements, joint recovery of the shape of the domain and conductivity are pursued in [12–15]. The inverse EIT problem with unknown anisotropic conductivity tensor as in (1.3) is highly ill-posed, and even with a perfect Dirichlet to Neumann map there is a non-uniqueness [16]. This is the structural non-uniqueness, and one can talk about the identification of the conductivity tensor up to diffeomorphisms which keep the boundary fixed [11, 16–21]. An alternative approach is based on imposing apriori structural constraints on the class of anisotropies [22–28].

Inverse EIT Problem is more difficult than Calderon's problem due to the fact that the infinite-dimensional conductivity function σ (or tensor A) and finite-dimensional voltage vector U must be identified based on the finitely many boundary electrode voltage measurements. The input data is a finite-dimensional current vector, whereas in Calderon's problem input data is given through infinite-dimensional boundary operator "Dirichlet-to-Neuman" or "Neuman-to-Dirichlet". Therefore, the inverse EIT problem is highly ill-posed, and powerful regularization methods are required for its solution. It is essential to note that the size of the input current vector is limited to the number of electrodes, and there is no flexibility to increase its size. It would be natural to suggest that the multiple data sets - input currents can be implemented for the identification of the same conductivity function. However, note that besides the unknown conductivity function, there is an unknown boundary voltage vector with a size directly proportional to the size of the input current vector. Accordingly, multiple experiments with "current-to-voltage" measurements are not reducing underdeterminacy of the inverse problem. One can prove uniqueness and stability results by restricting isotropic conductivity to the finite-dimensional subset of piecewise analytic functions provided that the number of electrodes is

large enough [29, 30]. Within the last three decades, many methods developed for the numerical solution of the ill-posed inverse EIT problem both in isotropic and anisotropic conductivities. Without any ambition to present a full review, we refer to some significant developments such as recovery of the small inclusions from boundary measurements [31, 32]; hybrid conductivity imaging methods [33–35]; multi-frequency EIT imaging methods [36, 37]; finite element and adaptive finite element method [38, 39]; imaging algorithms based on the sparsity reconstruction [36, 40]; globally convergent method for shape reconstruction in EIT [41]; D-bar method, diction reconstruction method, recovering boundary shape and imaging the anisotropic electrical conductivity [42–46]; globally convergent regularization method using Carleman weight function [47].

Inverse EIT problem was widely studied in the framework of Bayesian statistics [48]. In [49] inverse EIT problem is formulated as a Bayesian problem of statistical inference and the Markov Chain Monte Carlo method with various prior distributions is implemented for calculation of the posterior distributions of the unknown parameters conditioned on measurement data. In [50] Bayesian model of the regularized version of the inverse EIT problem is analyzed. In [51] the Bayesian method with Whittle-Matérn priors is applied to the inverse EIT problem. In general, the strategy of the Bayesian approach to the inverse EIT problem in the infinite-dimensional setting is twofold. The first approach is based on discretization followed by the application of finite-dimensional Bayesian methods. All the described papers followed this approach, which is outlined in [48]. The alternative approach is based on direct application of the Bayesian methods in functional spaces before discretization [52, 53].

The goal of the paper is to introduce a variational formulation of the inverse EIT problem as a PDE constrained optimal control problem in a Besov space. The novelty of the control-theoretic model is its adaptation to the clinical situations when additional "voltage-to-current" measurements can increase the size of the input data from the number of electrodes m up to $m!$ while keeping the size of the unknown parameters fixed. Our method theoretically applies to both isotropic and anisotropic conductivities. Therefore, we pursue the anisotropic case in theoretical analysis, although numerical results are demonstrated only in the isotropic case. We prove the existence of the optimal control and Fréchet differentiability in the Besov space setting. The formula for the Fréchet gradient and optimality condition is derived. Based on the Fréchet differentiability result we develop a projective gradient method in Besov spaces. Extensive numerical analysis in the 2D case by implementing the projective gradient method, re-parameterization via PCA, and Tikhonov regularization is pursued. Numerical analysis of the simulated model example in the 2D case demonstrates that by increasing the number of boundary input currents from m to m^2 through additional "voltage-to-current" measurements the resolution of the electrical conductivity of the body identified via gradient method in Besov space framework is significantly improved. The organization of the paper is as follows. In Section 2 we introduce the notations of the functional spaces. In Section 3 we introduce the Inverse EIT Problem as PDE constrained optimal control problem. In Section 4 we formulate the main results. Proofs of the main results are presented in Section 5. In Section 6 we present the results of the computational analysis for the 2D model. Finally, in Section 7 we outline the main conclusions.

2. Notations

In this section, assume Q is a domain in $\mathbb{R}^n$.

- For $1 \leq p < \infty$, $L_p(Q)$ is a Banach space of measurable functions on Q with finite norm

$$\|u\|_{L_p(Q)} := \Big(\int_Q |u(x)|^p dx\Big)^{\frac{1}{p}}.$$

In particular if $p = 2$, $L_2(Q)$ is a Hilbert space with inner product

$$(f,g)_{L_2(Q)} = \int_Q f(x)g(x)dx$$

- $L_\infty(Q)$ is a Banach space of measurable functions on Q with finite norm

$$\|u\|_{L_\infty(Q)} := \operatorname*{ess\,sup}_{x\in Q} |u(x)|$$

- For $s \in \mathbb{Z}_+$, $W_p^s(Q)$ is the Banach space of measurable functions on Q with finite norm

$$\|u\|_{W_p^s(Q)} := \Big(\int_Q \sum_{|\alpha|\le s} |D^\alpha u(x)|^p dx\Big)^{\frac{1}{p}}$$

where $\alpha = (\alpha_1, \alpha_2, ..., \alpha_n)$, α_j are nonnegative integers, $|\alpha| = \alpha_1 + ... + \alpha_n$, $D_k = \frac{\partial}{\partial x_k}$, $D^\alpha = D_1^{\alpha_1} ... D_n^{\alpha_n}$. In particular if $p = 2$, $H^s(Q) := W_2^s(Q)$ is a Hilbert space with inner product

$$(f,g)_{H^s(Q)} = \sum_{|\alpha|\le s} (D^\alpha f(x), D^\alpha g(x))_{L_2(Q)}$$

- For $s \notin \mathbb{Z}_+$, $B_p^s(Q)$ is the Banach space of measurable functions on Q with finite norm

$$\|u\|_{B_p^s(Q)} := \|u\|_{W_p^{[s]}(Q)} + [u]_{B_p^s(Q)}$$

where

$$[u]_{B_p^s(Q)} := \int_Q \int_Q \frac{\big|\frac{\partial^{[s]}u(x)}{\partial x^{[s]}} - \frac{\partial^{[s]}u(y)}{\partial x^{[s]}}\big|^p}{|x-y|^{1+p(s-[s])}} dxdy\Big)^{\frac{1}{p}}$$

and $H^\varepsilon(Q) := B_2^\varepsilon(Q)$ is an Hilbert space.

- $\mathbf{ba}(Q) = \big(L_\infty(Q)\big)'$ is the Banach space of bounded and finitely additive signed measures on Q and the dual space of $L_\infty(Q)$ with finite norm

$$\|\phi\|_{\mathbf{ba}(Q)} = |\phi|(Q),$$

$|\phi|(Q)$ is total variation of ϕ and defined as $|\phi|(Q) = \sup \sum_i \phi(E_i)$, where the supremum is taken over all partitions $\cup E_i$ of E into measurable subsets E_i.

- $\mathbb{M}^{m\times n}$ is a space of real $m \times n$ matrices.
- $\mathscr{L} := L_\infty(Q; \mathbb{M}^{n\times n})$ is the Banach space of $n \times n$ matrices of $L_\infty(Q)$ functions.
- $\mathscr{L}' := \mathbf{ba}(Q; \mathbb{M}^{n\times n}) = \big(L_\infty(Q; \mathbb{M}^{n\times n})\big)'$ is the Banach space of $n \times n$ matrices of $\mathbf{ba}(Q)$ measures.

3. Optimal control problem

We formulate Inverse EIT Problem as the following PDE constrained optimal control problem. Given electrode current pattern I and corresponding electrode voltage measurement vector U^*, consider the minimization of the cost functional

$$\mathscr{J}(v) = \sum_{l=1}^{m} \Big| \int_{E_l} \frac{U_l - u(x)}{Z_l} ds - I_l \Big|^2 + \beta |U - U^*|^2 \tag{3.1}$$

on the control set

$$V_R = \Big\{ v = (A,U) \in \Big(L_\infty(Q;\mathbb{M}^{n\times n}) \bigcap H^\varepsilon(Q;\mathbb{M}^{n\times n}) \Big) \times \mathbb{R}^m \Big| \sum_{l=1}^{m} U_l = 0,$$
$$\|A\|_{L_\infty} + \|A\|_{H^\varepsilon} + |U| \le R,\ \xi^T A \xi \ge \mu |\xi|^2,\ \forall \xi \in \mathbb{R}^n,\ \mu > 0 \Big\}$$

where $\beta > 0$, and $u = u(\cdot;v) \in H^1(Q)$ is a solution of the elliptic problem (1.3)–(1.5). This optimal control problem will be called Problem $\mathscr{J}$. The first term in the cost functional $\mathscr{J}(v)$ characterizes the mismatch of the condition (1.6) in light of the Robin condition (1.5).

Note that the variational formulation of the EIT Problem is a particular case of the Problem $\mathscr{J}$, when the conductivity tensor A is known, and therefore is removed from the control set by setting $R = +\infty$ and $\beta = 0$:

$$\mathscr{I}(U) = \sum_{l=1}^{m} \Big| \int_{E_l} \frac{U_l - u(x)}{Z_l} ds - I_l \Big|^2 \to \inf \tag{3.2}$$

in a control set

$$W = \Big\{ U \in \mathbb{R}^m \Big| \sum_{l=1}^{m} U_l = 0 \Big\} \tag{3.3}$$

where $u = u(\cdot;v) \in H^1(Q)$ is a solution of the elliptic problem (1.3)–(1.5). This optimal control problem will be called Problem $\mathscr{I}$. It is a convex PDE constrained optimal control problem (Remark 1, Section 4).

Inverse EIT problem on the identification of the electrical conductivity tensor A with m input data $(I_l)_{l=1}^m$ is highly ill-posed. Optimal control Problem $\mathscr{J}$ inherits ill-posedness of the inverse EIT problem. Next, we formulate an optimal control problem which is adapted to the situation when the size of the input data can be increased through additional measurements while keeping the size of the unknown parameters fixed. Let $I^1 := I$ is a current pattern input, and $U^1 = (U_1, ..., U_m)$ is a corresponding boundary electrode voltage measurements. Consider $m-1$ new permutations of boundary voltages

$$U^j = (U_j, ..., U_m, U_1, ..., U_{j-1}),\ j = 2, ..., m \tag{3.4}$$

applied to electrodes $E_1, E_2, \ldots, E_m$ respectively. Assume that the "voltage–to–current" measurement allows us to measure associated currents $I^j = (I_1^j, \ldots, I_m^j)$. By setting $U^1 = U^*$ and having a new set of m^2 input data $(I^j)_{j=1}^m$, we now consider optimal control problem on the minimization of the new cost functional

$$\mathscr{K}(v) = \sum_{j=1}^{m} \sum_{l=1}^{m} \Big| \int_{E_l} \frac{U_l^j - u^j(x)}{Z_l} ds - I_l^j \Big|^2 + \beta |U - U^*|^2 \tag{3.5}$$

on a control set V_R, where each function $u^j(\cdot;A,U^j), j=1,...,m$, solves elliptic PDE problem (1.3)–(1.5) with U replaced by U^j. This optimal control problem will be called Problem $\mathscr{K}$. Note that the number of input currents in the Problem $\mathscr{K}$ has increased from m to m^2. However, the size of unknown control vector is unchanged, and in particular there are only m unknown voltages $U_1,\dots,U_m$, whereas all vectors $U^j, j=2,...,m$, are formed by their permutation as in (3.4). The price we pay for this gain is the increase of the number of PDE constraints, which has increased from 1 to m. It should be noted that similar approach can be pursued to increase the size of input data up to $m!$ by adding possible permutations of U in (3.4).

We effectively use Problem $\mathscr{I}$ to generate model examples of the inverse EIT problem which adequately represents the diagnosis of the cancerous tumor in reality. Computational analysis based on the Fréchet differentiability result and gradient method in Besov spaces for the Problems $\mathscr{J}$ and $\mathscr{K}$ is pursued in realistic model examples.

4. Main results

Let bilinear form $B: H^1(Q)\times H^1(Q)\to\mathbb{R}$ be defined as

$$B[u,\eta]=\int_Q\sum_{i,j=1}^n a_{ij}u_{x_j}\eta_{x_i}dx+\sum_{l=1}^m\frac{1}{Z_l}\int_{E_l}u\eta ds. \tag{4.1}$$

Definition 4.1. For a given $v\in V_R$, $u=u(\cdot;v)\in H^1(Q)$ is called a solution of the problem (1.3)–(1.5) if

$$B[u,\eta]=\sum_{l=1}^m\frac{1}{Z_l}\int_{E_l}\eta U_l ds,\quad \forall\eta\in H^1(Q). \tag{4.2}$$

For a given control vector $v\in V_R$ and corresponding $u(\cdot;v)\in H^1(Q)$, consider the adjoined problem:

$$\sum_{ij}(a_{ij}\psi_{x_i})_{x_j}=0, \qquad x\in Q \tag{4.3}$$

$$\frac{\partial\psi}{\partial\mathscr{N}}=0, \qquad x\in\partial Q-\bigcup_{l=1}^m E_l \tag{4.4}$$

$$\psi+Z_l\frac{\partial\psi}{\partial\mathscr{N}}=2\int_{E_l}\frac{u-U_l}{Z_l}ds+2I_l,\quad x\in E_l,\ l=\overline{1,m} \tag{4.5}$$

Definition 4.2. $\psi\in H^1(Q)$ is called a solution of the adjoined problem (4.3)–(4.5) if

$$B[\psi,\eta]=\sum_l\int_{E_l}\frac{\eta}{Z_l}\Big[2\int_{E_l}\frac{u-U_l}{Z_l}ds+2I_l\Big]ds,\ \forall\eta\in H^1(Q). \tag{4.6}$$

In Lemma 5.1, Section 5 it is demonstrated that for a given $v\in V_R$, both elliptic problems are uniquely solvable.

Definition 4.3. Let V be a convex and closed subset of the Banach space H. We say that the functional $\mathscr{J}: V\to\mathbb{R}$ is differentiable in the sense of Fréchet at the point $v\in V$ if there exists an element $\mathscr{J}'(v)\in H'$ of the dual space such that

$$\mathscr{J}(v+h)-\mathscr{J}(v)=\big\langle\mathscr{J}'(v),h\big\rangle_H+o(h,v) \tag{4.7}$$

where $v+h \in V \cap \{u : \|u\| < \gamma\}$ for some $\gamma > 0$; $\langle \cdot, \cdot \rangle_H$ is a pairing between H and its dual H', and

$$\frac{o(h,v)}{\|h\|} \to 0, \quad \text{as } \|h\| \to 0.$$

The expression $d\mathscr{J}(v) = \langle \mathscr{J}'(v), \cdot \rangle_H$ is called a Fréchet differential of $\mathscr{J}$ at $v \in V$, and the element $\mathscr{J}'(v) \in H'$ is called Fréchet derivative or gradient of $\mathscr{J}$ at $v \in V$.

Note that if Fréchet gradient $\mathscr{J}'(v)$ exists at $v \in V$, then the Fréchet differential $d\mathscr{J}(v)$ is uniquely defined on a convex cone ([55–61])

$$\mathscr{H}_v = \{w \in H : w = \lambda(u-v), \lambda \in [0,+\infty), u \in V\}.$$

The following are the main results of the paper:

Theorem 4.4. *(Existence of an Optimal Control). Problem $\mathscr{J}$ has a solution, i.e.,*

$$V_* = \{v = (A,U) \in V_R; \mathscr{J}(v) = \mathscr{J}_* = \inf_{v \in V_R} \mathscr{J}(v)\} \neq \emptyset. \tag{4.8}$$

Theorem 4.5. *(Fréchet Differentiability): The functional $\mathscr{J}(v)$ is differentiable on V_R in the sense of Fréchet; the Fréchet differential $d\mathscr{J}(v)$ and the gradient $\mathscr{J}'(A,U) \in \mathscr{L}' \times \mathbb{R}^m$ are*

$$\begin{aligned} \langle \mathscr{J}'(v), \delta v \rangle_H &= -\int_Q \sum_{i,j=1}^n u_{x_j} \psi_{x_i} \delta a_{ij} dx \\ &+ \sum_{k=1}^m \Big(\sum_{l=1}^m 2\Big[\int_{E_l} \frac{U_l - u}{Z_l} ds - I_l\Big] \int_{E_l} \frac{1}{Z_l} (\delta_{lk} - w^k(s)) ds + 2\beta(U_k - U_k^*) \Big) \delta U_k, \end{aligned} \tag{4.9}$$

$$\begin{aligned} \mathscr{J}'(A,U) &= \Big(\mathscr{J}'_A(A,U), \mathscr{J}'_U(A,U) \Big) \\ &= \left(-\big(\psi_{x_i} u_{x_j}\big)_{i,j=1}^n, \Big(\sum_{l=1}^m 2\Big[\int_{E_l} \frac{U_l - u}{Z_l} ds - I_l\Big] \int_{E_l} \frac{1}{Z_l} (\delta_{lk} - w^k(s)) ds + 2\beta(U_k - U_k^*) \Big)_{k=1}^m \right) \end{aligned} \tag{4.10}$$

where $u = u(\cdot; v), \psi = \psi(\cdot; v)$; $w^k = \frac{\partial u}{\partial U_k} = u(\cdot; A, e_k)$, $k = 1,2,..,m$, is a solution of (1.3)–(1.5) *with $v = (A, e_k)$, $e_k \in \mathbb{R}$ is a unit vector in x_k-direction; δ_{lk} is a Kronecker delta; $\delta v = (\delta A, \delta U) = ((\delta a_{ij})_{i,j=1}^n, (\delta U_k)_{k=1}^m)$ is a variation of the control vector $v \in V_R$ such that $v + \delta v \in V_R$.*

Corollary 1. *(Optimality Condition) If $v \in V_R$ is an optimal control in Problem $\mathscr{J}$, then the following variational inequality is satisfied:*

$$\langle \mathscr{J}'(\boldsymbol{v}), v - \boldsymbol{v} \rangle_H \geq 0, \ \forall v \in V_R. \tag{4.11}$$

Corollary 2. *(Fréchet Differentiability): The functional $\mathscr{K}(v)$ is differentiable on V_R in the sense of Fréchet and the Fréchet gradient $\mathscr{K}'(\sigma, U) \in \mathscr{L}' \times \mathbb{R}^m$ is*

$$\mathscr{K}'(v) = \Big(\mathscr{K}'_A(A,U), \mathscr{K}'_U(A,U) \Big) =$$

$$\left(-\Big(\sum_{j=1}^{m}\psi^j_{x_p}u^j_{x_q}\Big)^n_{p,q=1},\Big(\sum_{j=1}^{m}\sum_{l=1}^{m}2\Big[\int_{E_l}\frac{U_l^j-u_j}{Z_l}ds-I_l^j\Big]\int_{E_l}\frac{\delta_{l,\theta_{kj}}-w^{\theta_{kj}}(s)}{Z_l}ds+2\beta(U_k-U_k^*)\Big)^m_{k=1}\right) \tag{4.12}$$

where $\psi^j(\cdot), j=1,...,m$, *be a solution of the adjoined PDE problem* (4.3)–(4.5) *with* $u(\cdot), U$ *and* I *replaced with* $u^j(\cdot), U^j$, I^j *respectively, and*

$$\theta_{kj}=\begin{cases}k-j+1, & \text{if } j\le k,\\ m+k-j+1, & \text{if } j>k.\end{cases}$$

Remark 1. Existence and uniqueness of the solution to the EIT problem (1.2)–(1.6) is established in [2]. Note that if $(\hat{u},\hat{U})$ is a solution of the EIT Problem (1.2)–(1.6), then $\hat{U}$ is a minimizer of the Problem $\mathscr{I}$ with minimum value $\mathscr{I}(\hat{U})=0$, and $\hat{u}$ is a corresponding optimal state vector solving (1.3)–(1.5) with $U=\hat{U}$. Functional (3.2) in the optimal control Problem $\mathscr{I}$ is convex due to the following formula

$$\mathscr{I}(\alpha U^1+(1-\alpha)U^2)=\alpha\mathscr{I}(U^1)+(1-\alpha)\mathscr{I}(U^2)-\alpha(1-\alpha)\sum_{l=1}^{m}Z_l^{-2}\Big|\int_{E_l}(U_l^1-U_l^2-u^1+u^2)ds\Big|^2$$

where $U^1,U^2\in W,\alpha\in[0,1];u^i=u(\cdot;U^i),i=1,2$ is a solution of (1.3)–(1.5) with $U=U^i$.Therefore, Problem $\mathscr{I}$ is a convex minimization problem with a unique global minimizer $\hat{U}$.

4.1. Gradient Method in Banach Space

Fréchet differentiability result of Theorem 4.5 and the formula (4.10) for the Fréchet derivative suggest the following algorithm based on the projective gradient method in Banach space H for the Problem $\mathscr{J}$.

Step 1. Set $N=0$ and choose initial vector function $(A^0,U^0)\in V_R$ where

$$A^0=(a^0_{ij})^n_{ij=1},\qquad U^0=(U^0_1,...,U^0_m),\qquad \sum_{l=0}^{m}U_l^0=0.$$

Step 2. Solve the PDE problem (1.3)–(1.5) to find $u^N=u(\cdot;A^N,U^N)$ and $\mathscr{J}(A^N,U^N)$.

Step 3. If $N=0$, move to Step 4. Otherwise, check the following criteria:

$$\left|\frac{\mathscr{J}(A^N,U^N)-\mathscr{J}(A^{N-1},U^{N-1})}{\mathscr{J}(A^{N-1},U^{N-1})}\right|<\varepsilon,\quad \frac{\|A^N-A^{N-1}\|}{\|A^{N-1}\|}<\varepsilon,\ \frac{|U^N-U^{N-1}|}{|U^{N-1}|}<\varepsilon \tag{4.13}$$

where ε is the required accuracy. If the criteria are satisfied, then terminate the iteration. Otherwise, move to Step 4.

Step 4. Solve the PDE problem (1.3)–(1.5) to find $w^N_k=u(\cdot;A^N,e_k),k=1,...,m$.

Step 5. Solve the adjoined PDE problem (4.3)–(4.5) to find $\psi_N=\psi(\cdot;A^N,U^N,u^N)$.

Step 6. Choose stepsize parameter $\alpha_N > 0$ and compute a new control vector components $\tilde{A}^{N+1} = (\tilde{a}_{ij}^{N+1}(x))_{i,j=1}^{n}, \tilde{U}^{N+1} \in \mathbb{R}^m$ as follows:

$$\tilde{a}_{ij}^{N+1}(x) = a_{ij}^N(x) + \alpha_N \psi_{x_i}^N u_{x_j}^N,\ i,j = 1,...,n, \tag{4.14}$$

$$\tilde{U}_k^{N+1} = U_k^N - \alpha_N \Big[\sum_{l=1}^{m} 2\Big(\int_{E_l} \frac{U_l^N - u^N(s)}{Z_l} ds - I_l \Big) \int_{E_l} \frac{1}{Z_l} (\delta_{lk} - w_k^N(s)) ds + 2\beta (U_k^N - U_k^*) \Big],\ k = 1,...,m. \tag{4.15}$$

Step 7. Replace $(\tilde{A}^{N+1}, \tilde{U}^{N+1})$ with $(A^{N+1}, U^{N+1}) \in V_R$ as follows

$$a_{ij}^{N+1}(x) = \begin{cases} \mu, & if\ \tilde{a}_{ij}^{N+1}(x) \le \mu, \\ \tilde{a}_{ij}^{N+1}(x), & if\ \mu \le \tilde{a}_{ij}^{N+1}(x) \le R, \\ R, & if\ \tilde{a}_{ij}^{N+1}(x) > R, \end{cases} \tag{4.16}$$

$$U_k^{N+1} = \tilde{U}_k^{N+1} - \frac{1}{m} \sum_{k=1}^{m} \tilde{U}_k^{N+1},\ k = 1,...,m. \tag{4.17}$$

Then replace N with $N+1$ and move to Step 2.

Based on formula (4.12) similar algorithm is implemented for solving Problem $\mathscr{K}$.

Remark 2. Corresponding differentiability and optimality results of Theorem 4.5 and Corollary 1 can be easily established for Problem $\mathscr{I}$, and the gradient $\mathscr{I}_U'$ coincides with $\mathscr{J}_U'$ from (4.10). Similar algorithm for the iterative gradient method for the identification of $U \in \mathbb{R}^m$ can be developed for the Problem $\mathscr{I}$.

4.2. Increase of input data for simulations and clinical applications

The new optimal control framework for the inverse EIT problem and the results outlined in Sections 3, 4 suggest the following multi-stage algorithm with the increase of data both in simulations, as well as in clinical applications.

Stage 1. *Simulation:* By selecting boundary current pattern $I = (I_l)_{l=1}^m$ and electrical conductivity matrix $A_{true} = (a_{ij})$ we simulate the EIT model example with $A = A_{true}$ by solving convex minimization Problem $\mathscr{I}$, and find its unique minimizer $U^* \in W$. We then simulate inverse EIT problem with true solution (A_{true}, U_{true}), where U_{true} is identified with U^*.

Clinical Application: Implement the "current–to–voltage" procedure: by injecting current pattern $I = (I_l)_{l=1}^m$ on the electrodes E_l, $l = 1,\ldots,m$, take the measurement of the voltages $U^* = (U_1^*,\ldots,U_m^*)$.

Stage 2. *Simulation & Clinical Application:* Solve the optimal control Problem $\mathscr{J}$ with m input data $I = (I_l)_{l=1}^m$ by the gradient descent method described in Section 4.1, and recover optimal control $(\sigma_{true}, U_{true})$. If precision and accuracy is not satisfactory, move to next stage to increase the input data without affecting optimal control.

Stage 3. *Simulation:* To increase the size of input data from m to m^2 we apply the same set of boundary voltages U_l^* to different electrodes E_l using a "rotation scheme", i.e., we denote $U^1 = U^*$, $I^1 = I$ and consider $m-1$ new permutations of boundary voltages as in (3.4) applied to electrodes

$E_1, E_2, \ldots, E_m$ respectively. For each boundary voltage vector U^j we solve elliptic PDE problem (6.1)–(6.3) to obtain the distribution of electrical potential $u_j(\cdot) = u(\cdot; U^j)$ over boundary ∂Q. By using "voltage–to–current" formula (6.4), we calculate current pattern I^j associated with U^j. Thus, a new set $(I^j)_{j=1}^m$ contains m^2 input data. Then we solve Problem $\mathscr{K}$ with extended data set by the gradient descent method described in Section 4.1, and recover an optimal control $(\sigma_{true}, U_{true})$. **Note that despite increase of the input data from m to m^2, $(\sigma_{true}, U_{true})$ is still an optimal control in Problem $\mathscr{K}$.**

Clinical Application: To increase the size of input data from m to m^2, we implement "voltage–to–current" procedure: by injecting $m-1$ new sets of voltages U^j, $j = 2, ..., m$, from (3.4) on the electrodes E_l, $l = 1, \ldots, m$, take the measurement of the currents $I^j = (I_1^j, \ldots, I_m^j)$. Then as in *Simulation* we solve Problem $\mathscr{K}$ with extended data set, and recover an optimal control $(\sigma_{true}, U_{true})$.

Stage 3 can be repeated to increase the size of the input data from m up to $m!$ while keeping the optimal control unchanged. Precisely, one can apply any set of permutations of U^* to electrodes, and implement "voltage–to–current" measurements to deduce the corresponding set of electrode current vectors, and solve the Problem $\mathscr{K}$ to find an optimal control $(\sigma_{true}, U_{true})$.

5. Proofs of the main results

Well-posedness of the elliptic problems (1.3)–(1.5) and (4.3)–(4.5) follow from the Lax-Milgram theorem [54].

Lemma 5.1. *For $\forall v \in V_R$ there exists a unique solution $u = u(\cdot, v) \in H^1(Q)$ to the problem* (1.3)–(1.5) *which satisfy the energy estimate*

$$\|u\|^2_{H^1(Q)} \leq C \sum_{l=1}^{m} Z_l^{-2} U_l^2. \tag{5.1}$$

Proof: *Step 1. Introduction of the equivalent norm in $H^1(Q)$.* Let

$$|||u|||_{H^1(Q)} := \left[\int_Q |\nabla u|^2 dx + \sum_{l=1}^{m} \int_{E_l} u^2 ds \right]^{\frac{1}{2}}, \tag{5.2}$$

and prove that this is equivalent to the standard norm of $H^1(Q)$, i.e., there is $c > 1$ such that $\forall u \in H^1(Q)$

$$c^{-1} \|u\|_{H^1(Q)} \leq |||u|||_{H^1(Q)} \leq c \|u\|_{H^1(Q)}. \tag{5.3}$$

The second inequality immediately follows due to bounded embedding $H^1(Q) \hookrightarrow L^2(\partial Q)$ ([54]). To prove the first inequality assume on the contrary that

$$\forall k > 0, \quad \exists u_k \in H^1(Q) \quad \text{such that } \|u_k\|_{H^1(Q)} > k |||u_k|||_{H^1(Q)}.$$

Without loss of generality, we can assume that $\|u_k\| = 1$, and therefore

$$\|\nabla u_k\|_{L_2(Q)} \longrightarrow 0, \ \|u_k\|_{L_2(E_l)} \longrightarrow 0, \quad \text{as } k \to \infty, \quad l = 1, 2, ...m. \tag{5.4}$$

Since $\{u_k\}$ is a bounded sequence in $H^1(Q)$, it is weakly precompact in $H^1(Q)$ and strongly precompact in both $L_2(Q)$ and $L_2(\partial Q)$ ([62–64]). Therefore, there exists a subsequence $\{u_{k_j}\}$ and $u \in H^1(Q)$ such

that u_{k_j} converges to u weakly in $H^1(Q)$ and strongly in $L_2(Q)$ and $L_2(\partial Q)$. Without loss of generality, we can assume that the whole sequence $\{u_k\}$ converges to u. From the first relation of (5.4) it follows that ∇u_k converges to zero strongly, and therefore also weakly in $L^2(Q)$. Due to uniqueness of the limit, $\nabla u = 0$, and therefore $u = const$ a.e. in Q, and on the ∂Q in the sense of traces. According to the second relation in (5.4), and since $|E_l| > 0$, it follows that $const = 0$. This fact contradicts with $\|u_k\| = 1$, and therefore the second inequality is proved.

Step 2. Application of the Lax-Milgram theorem. Since $v \in V_R$, by using Cauchy-Bunyakowski-Schwartz (CBS) inequality, bounded trace embedding $H^1(Q) \hookrightarrow L^2(\partial Q)$ and (5.3) we have the following estimations for the bilinear form B:

$$|B[u,\eta]| \le \alpha \|u\|_{H^1(Q)} \|\eta\|_{H^1(Q)},\ B[u,u] \ge \beta \|u\|^2_{H^1(Q)} \tag{5.5}$$

where $\alpha, \beta > 0$ are independent of u, η. Note that the component U of the control vector v defines a bounded linear functional $\hat{U} : H^1(Q) \to \mathbb{R}$ according to the right-hand side of (4.2):

$$\hat{U}(\eta) := \sum_{l=1}^{m} \frac{U_l}{Z_l} \int_{E_l} \eta ds. \tag{5.6}$$

Indeed, by using CBS inequality and bounded trace embedding $H^1(Q) \hookrightarrow L^2(\partial Q)$ we have

$$|\hat{U}(\eta)| \le |Q|^{\frac{1}{2}} \big(\sum_{l=1}^{m} Z_l^{-2} U_l^2 \big)^{\frac{1}{2}} \|\eta\|_{L_2(\partial Q)} \le C \|\eta\|_{H^1(Q)}. \tag{5.7}$$

From (5.5), (5.7) and Lax-Milgram theorem ([54]) it follows that there exists a unique solution of the problem (1.3)–(1.5) in the sense of Definition 4.2.

Step 3. Energy estimate. By choosing η as a weak solution u in (4.2), using (1.7) and Cauchy's inequality with ε we derive

$$\mu \|\nabla u\|^2_{L_2(Q)} + z_0 \sum_{l=1}^{m} \|u\|^2_{L_2(E_l)} \le \frac{c}{\varepsilon} \sum_{l=1}^{m} Z_l^{-2} U_l^2 + \varepsilon |\partial Q| \sum_{l=1}^{m} \left(\int_{E_l} |u|^2 ds \right) \tag{5.8}$$

where $z_0 = \min\limits_{1 \le l \le m} Z_l^{-1}$. By choosing $\varepsilon = (2|\partial Q|)^{-1} z_0$ from (5.8) it follows that

$$|||u|||_{H^1(Q)} \le C \sum_{l=1}^{m} Z_l^{-2} U_l^2. \tag{5.9}$$

From (5.3) and (5.9), energy estimate (5.1) follows. Lemma is proved.■

Corollary 3. *For $\forall v \in V_R$ there exists a unique solution $\psi = \psi(\cdot, v) \in H^1(Q)$ of the adjoined problem* (4.3)–(4.5) *which satisfy the energy estimate*

$$\|\psi\|^2_{H^1(Q)} \le C \sum_{l=1}^{m} Z_l^{-2} \Big[\int_{E_l} \frac{U_l - u}{Z_l} ds - I_l \Big]^2 \tag{5.10}$$

where $u = u(\cdot; v) \in H^1(Q)$ is a solution of the problem (1.3)–(1.5) .

Proof of Theorem 4.4. Let $\{v_k\} = \{(A^k, U^k)\} \subset V_R$ be a minimizing sequence

$$\lim_{k\to\infty} \mathscr{J}(v_k) = \mathscr{J}_*.$$

Since $\{A^k\}$ is a bounded sequence in $H^\varepsilon(Q;\mathbb{M}^{n\times n})$, it is weakly precompact in $H^\varepsilon(Q;\mathbb{M}^{n\times n})$ and strongly precompact in $L_2(Q;\mathbb{M}^{n\times n})$ [62–64]. Therefore, there exists a subsequence $\{A^{k_p}\}$ which converges weakly in $H^\varepsilon(Q;\mathbb{M}^{n\times n})$ and strongly in $L_2(Q;\mathbb{M}^{n\times n})$ to some element $A \in H^\varepsilon(Q;\mathbb{M}^{n\times n})$. Since any strong convergent sequence in $L_2(Q;\mathbb{M}^{n\times n})$ has a subsequence which converges a.e. in Q, without loss of generality one can assume that the subsequence A^{k_p} converges to A a.e. in Q, which implies that $A \in L_\infty(Q;\mathbb{M}^{n\times n}) \cap H^\varepsilon(Q;\mathbb{M}^{n\times n}) \cap V_R$. Since U^k is a bounded sequence in $\mathbb{R}^m$ it has a subsequence which converges to some $U \in \mathbb{R}^m, |U| \le R$. Without loss of generality we can assume that the whole minimizing sequence $v_k = (A_k, U^k)$ converges $v = (A,U) \in V_R$ in the indicated way.

Let $u_k = u(x;v_k)$, $u = u(x;v) \in H^1(Q)$ are weak solutions of (1.3)–(1.5) corresponding to v_k and v respectively. By Lemma 5.1 u_k satisfy the energy estimate (5.1) with U^k on the right hand side, and therefore it is uniformly bounded in $H^1(Q)$. By the Rellich-Kondrachov compact embedding theorem there exists a subsequence $\{u_{k_p}\}$ which converges weakly in $H^1(Q)$ and strongly in both $L_2(Q)$ and $L_2(\partial Q)$ to some function $\tilde{u} \in H^1(Q)$([62–64]). Without loss of generality assume that the whole sequence u_k converges to $\tilde{u}$ weakly in $H^1(Q)$ and strongly both in $L_2(Q)$ and $L_2(\partial Q)$. For any fixed $\eta \in C^1(Q)$ weak solution u_k satisfies the following integral identity

$$\int_Q \sum_{i,j=1}^n a_{ij}^k u_{k_{x_j}} \eta_{x_i} dx + \sum_{l=1}^m \frac{1}{Z_l} \int_{E_l} u_k \eta ds = \sum_{l=1}^m \frac{1}{Z_l} \int_{E_l} \eta U_l^k ds. \tag{5.11}$$

Due to weak convergence of ∇u_k to $\nabla\tilde{u}$ in $L_2(Q;\mathbb{R}^n)$, strong convergence of u_k to $\tilde{u}$ in $L_2(\partial Q)$, strong convergence of a_{ij}^k to a_{ij} in $L_2(Q)$ and convergence of U^k to U, passing to the limit as $k \to \infty$, from (5.11) it follows

$$\int_Q \sum_{i,j=1}^n a_{ij} \tilde{u}_{x_j} \eta_{x_i} dx + \sum_{l=1}^m \frac{1}{Z_l} \int_{E_l} \tilde{u} \eta ds = \sum_{l=1}^m \frac{1}{Z_l} \int_{E_l} \eta U_l ds. \tag{5.12}$$

Due to density of $C^1(Q)$ in $H^1(Q)$ ([62–64]) the integral identity (5.12) is satisfied for arbitrary $\eta \in H^1(Q)$. Hence, $\tilde{u}$ is a weak solution of the problem (1.3)–(1.5) corresponding to the control vector $v = (A,U) \in V_R$. Due to uniqueness of the weak solution it follows that $\tilde{u} = u$, and the sequence u_k converges to the weak solution $u = u(x;v)$ weakly in $H^1(Q)$, and strongly both in $L_2(Q)$ and $L_2(\partial Q)$. The latter easily implies that

$$\mathscr{J}(v) = \lim_{n\to\infty} \mathscr{J}(v_n) = \mathscr{J}_*.$$

Therefore, $v \in V_*$ is an optimal control and (4.8) is proved. ■

Proof of Theorem 4.5. Let $v = (A,U) \in V_R$ is fixed and $\delta v = (\delta A, \delta U)$ is an increment such that $\bar{v} = v + \delta v \in V_R$ and $u = u(\cdot;v), \bar{u} = u(\cdot; v+\delta v) \in H^1(Q)$ are respective weak solutions of the problem (1.3)–(1.5). Since $u(\cdot;A,U)$ is a linear function of U it easily follows that

$$w^k = \frac{\partial u}{\partial U_k} = u(\cdot;A,e_k) \in H^1(Q),\ k = 1,2,..,m$$

is a solution of (1.3)–(1.5) with $v = (A, e_k)$, $e_k \in \mathbb{R}^m$ is a unit vector in x_k-direction. Straightforward calculation imply that

$$\frac{\partial \mathscr{J}}{\partial U_k} = \sum_{l=1}^{m} 2\Big[\int_{E_l} \frac{U_l - u}{Z_l} ds - I_l\Big] \int_{E_l} \frac{1}{Z_l}(\delta_{lk} - w^k) ds + 2\beta(U_k - U_k^*),\ k = 1, ..., m.$$

where δ_{lk} is a Kronecker delta.

In order to prove the Fréchet differentiability with respect to A, assume that $\delta U = 0$ and transform the increment of $\mathscr{J}$ as follows

$$\delta \mathscr{J} := \mathscr{J}(v + \delta v) - \mathscr{J}(v) = \sum_{l=1}^{m} \frac{1}{Z_l} \int_{E_l} 2\Big(\int_{E_l} \frac{u - U_l}{Z_l} ds + I_l\Big) \delta u ds + R_1, \tag{5.13}$$

$$R_1 = \sum_{l=1}^{m} Z_l^{-2} \Big(\int_{E_l} \delta u ds\Big)^2 \le \sum_{l=1}^{m} |E_l| Z_l^{-2} |||\delta u|||^2_{H^1(Q)} \tag{5.14}$$

where $\delta u = \bar{u} - u$. By subtracting integral identities (4.2) for $\bar{u}$ and u, and by choosing test function $\eta = \psi(\cdot; v)$ as a solution of the adjoined problem (4.3)–(4.5) we have

$$\int_Q \sum_{ij} \Big(\delta a_{ij} u_{x_j} + a_{ij}(\delta u)_{x_j} + \delta a_{ij}(\delta u)_{x_j}\Big) \psi_{x_i} dx + \sum_{l=1}^{m} \frac{1}{Z_l} \int_{E_l} \psi \delta u ds = 0. \tag{5.15}$$

By choosing $\eta = \delta u$ in the integral identity (4.6) for the weak solution ψ of the adjoined problem we have

$$-\int_Q \sum_{ij} a_{ij} \psi_{x_i} \delta u_{x_j} dx + \sum_l \int_{E_l} \frac{\delta u}{Z_l} \big[2 \int_{E_l} \frac{u - U_l}{Z_l} ds + 2I_l - \psi\big] ds = 0. \tag{5.16}$$

Adding (5.15) and (5.16) we derive

$$\sum_{l=1}^{m} \frac{1}{Z_l} \int_{E_l} 2\Big(\int_{E_l} \frac{u - U_l}{Z_l} dS(x) + I_l\Big) \delta u ds = \int_Q (-\sum_{ij} \delta a_{ij} u_{x_j} \psi_{x_i} - \sum_{ij} \delta a_{ij} (\delta u)_{x_j} \psi_{x_i}) dx. \tag{5.17}$$

From (5.13) and (5.17) it follows that

$$\delta \mathscr{J} = -\int_Q \sum_{ij} u_{x_j} \psi_{x_i} \delta a_{ij} dx + R_1 + R_2 \tag{5.18}$$

where

$$R_2 = -\int_Q \sum_{ij} \delta a_{ij} (\delta u)_{x_j} \psi_{x_i} dx. \tag{5.19}$$

To complete the proof it remains to prove that

$$R_1 + R_2 = o(\|\delta A\|_{L_\infty(Q; M^{n\times n})}) \quad \text{as } \|\delta A\|_{L_\infty(Q; M^{n\times n}} \to 0. \tag{5.20}$$

By subtracting integral identities (4.2) for $\bar{u}$ and u again, and by choosing test function $\eta = \delta u$ we have

$$\int_Q \sum_{ij} \bar{a}_{ij} (\delta u)_{x_j} (\delta u)_{x_i} dx + \sum_{l=1}^{m} \frac{1}{Z_l} \int_{E_l} (\delta u)^2 ds = -\int_Q \sum_{ij} \delta a_{ij} u_{x_j} (\delta u)_{x_i} dx. \tag{5.21}$$

By using positive definiteness of $\bar{A} \in V_R$ and by applying Cauchy inequality with $\varepsilon > 0$ to the right hand side, from (5.21) it follows that

$$\mu \int_Q |\nabla \delta u|^2 dx + \sum_{l=1}^{m} \frac{1}{Z_l} \int_{E_l} (\delta u)^2 ds \le \varepsilon \int_Q |\nabla \delta u|^2 dx + \frac{c}{\varepsilon} \int_Q |\sum_{ij} \delta a_{ij}|^2 |\nabla u|^2. \tag{5.22}$$

By choosing $\varepsilon = \mu/2$ and by applying the energy estimate (5.1) from (5.22) we derive

$$|||\delta u|||^2_{H^1(Q)} \le C \|\delta A\|^2_{L_\infty(Q;\mathbb{M}^{n\times n})}. \tag{5.23}$$

From (5.19) it follows that

$$|R_2| \le C \|\delta A\|_{L_\infty(Q;\mathbb{M}^{n\times n})} \|\nabla \delta u\|_{L_2(Q)} \|\nabla \psi\|_{L_2(Q)}. \tag{5.24}$$

From (5.1), (5.3), (5.10), (5.14), (5.23) and (5.24), desired estimation (5.20) follows. Theorem is proved.■

6. Numerical results

In this section we describe computational results for solving the Inverse EIT Problem in the 2D case ($n = 2$) according to the algorithm outlined in Section 4.1.

6.1. Computational model in 2D space

We pursue computational analysis of the inverse EIT problem with isotropic electrical conductivity tensor $A(x)$, i.e., $A(x) = \sigma(x)I$, where I is a 2×2 unit matrix. Problem $\mathscr{J}$ consists of minimization of the functional $\mathscr{J}(\sigma, U)$ defined in (3.1) on control set V_R, where $u = u(\cdot; \sigma, U)$ solves the elliptic PDE problem

$$\operatorname{div}(\sigma(x)\nabla u(x)) = 0, \qquad x \in Q \tag{6.1}$$

$$\frac{\partial u(x)}{\partial n} = 0, \qquad x \in \partial Q - \bigcup_{l=1}^{m} E_l \tag{6.2}$$

$$u(x) + Z_l \sigma(x) \frac{\partial u(x)}{\partial n} = U_l, \quad x \in E_l,\ l = \overline{1,m} \tag{6.3}$$

where n is an exterior unit normal vector on ∂Q. The first term in the cost functional $\mathscr{J}(\sigma, U)$ characterizes mismatch of the condition

$$\int_{E_l} \sigma(x) \frac{\partial u(x)}{\partial n} ds = I_l, \quad l = \overline{1,m} \tag{6.4}$$

in light of the Robin condition (6.3). We choose Q as a disk

$$Q = \left\{ x \in \mathbb{R}^2 :\ x_1^2 + x_2^2 < r_Q^2 \right\} \tag{6.5}$$

of radius $r_Q = 0.1$ with $m = 16$ equidistant electrodes E_l with half-width $w = 0.12$ rad covering approximately 61% of the boundary ∂Q as shown in Figure 1(a).

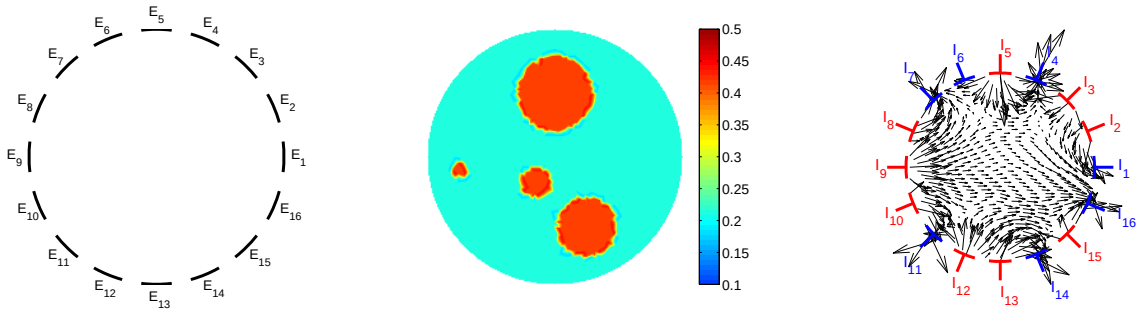

(a) (b) (c)

Figure 1. (a) Equispaced geometry of electrodes E_l placed over boundary ∂Q. (b) True electrical conductivity $\sigma_{true}(x)$. (c) Electrical currents I_l (positive in red, negative in blue) injected by electrodes E_l. Black arrows show the distribution of flux $\sigma(x)\nabla u(x)$ of the electrical potential u in the interior of domain Q.

Assume that the actual (true) electrical conductivity $\sigma_{true}(x)$ is given analytically as follows:

$$\sigma_{true}(x) = \begin{cases} 0.4, & x_1^2 + (x_2 - 0.05)^2 \le (0.03)^2 \\ 0.4, & (x_1 + 0.075)^2 + (x_2 + 0.01)^2 \le (0.0063)^2 \\ 0.4, & (x_1 + 0.015)^2 + (x_2 + 0.02)^2 \le (0.0122)^2 \\ 0.4, & (x_1 - 0.025)^2 + (x_2 + 0.055)^2 \le (0.0235)^2 \\ 0.2, & \text{otherwise} \end{cases} \tag{6.6}$$

It is measured in $(Ohm \cdot m)^{-1}$ and we set $\sigma_c = 0.4$ for cancer-affected parts (4 spots of different size) and $\sigma_h = 0.2$ to the remaining healthy part as it is demonstrated in Figure 1(b). Electrical currents I_l injected through electrodes E_l are outlined in Table 1 and shown schematically in Figure 1(c). Figure 1(c) shows the distribution of flux $\sigma(x)\nabla u(x)$ of the electrical potential u in the interior of domain Q corresponding to $\sigma_{true}(x)$.

Table 1. "Current–to–voltage" model parameters: electrical currents I_l injected by electrodes E_l, $l = 1, \ldots, 16$, with contact impedances Z_l, and initial guess for boundary voltages $U_{l,ini}$. The unit system used for all values is SI.

Electrode, l	1	2	3	4	5	6	7	8	9	10	11	12	13	14	15	16
$I_l \cdot 10^2$, A	-3	2	3	-7	6	-1	-4	2	4	3	-5	4	3	-5	2	-4
$Z_l \cdot 10^1$, Ohm	1	1	1	1	1	1	1	1	1	1	1	1	1	1	1	1
$U_{l,ini}$, V	-1	1	-1	1	-1	1	-1	1	-1	1	-1	1	-1	1	-1	1

Our optimization framework integrates computational facilities for solving state PDE problem (6.1)–(6.3), adjoint PDE problem (4.3)–(4.5), and evaluation of the Fréchet gradient according to (4.10), (4.12). These facilities are incorporated by using `FreeFem++` (see [66] for details), an open–source, high–level integrated development environment for obtaining numerical solutions of PDEs based on the Finite Element Method. To solve the PDE problem (6.1)–(6.3) numerically, spatial discretization is carried out by implementing triangular finite elements, P2 piecewise quadratic (continuous) representation for electrical potential $u(x)$ and P0 piecewise constant representation for conductivity field $\sigma(x)$. The system of algebraic equations obtained after such discretization is solved with `UMFPACK`, a solver for nonsymmetric sparse linear systems. The same technique is used for the numerical solution of the adjoint problem (4.3)–(4.5). All computations are performed using 2D domain Q (6.5) which is discretized using mesh $\mathscr{M}(n_v)$ created by specifying $n_v = 96$ vertices over boundary ∂Q and totaling 1996 triangular finite elements inside Q.

Unless otherwise stated, as an initial guess in the projective gradient algorithm described in Section 4.1 we choose a constant approximation to (6.6), given by $\sigma_{ini} = \frac{1}{2}(\sigma_h + \sigma_c) = 0.3$. Initial guess for boundary voltages is provided in Table 1 which is consistent with the ground potential condition (1.2). Determining the Robin part of the boundary conditions in (6.3) we equally set the electrode contact impedance $Z_l = 0.1$. The iterative optimization algorithm is performed by the Sparse Nonlinear OPTimizer `SNOPT`, a software package for solving large-scale nonlinear optimization problems [65]. It employs a sparse sequential quadratic programming (SQP) algorithm with limited-memory quasi-Newton approximations to the Hessian of the Lagrangian. This makes `SNOPT` especially effective for nonlinear problems with computationally expensive functionals and gradients. We set a termination conditions for `SNOPT` according to $\left|\frac{\mathscr{J}^N - \mathscr{J}^{N-1}}{\mathscr{J}^{N-1}}\right| < 10^{-6}$ or maximum number of optimization iterations $N_{max} = 250$, whichever comes first.

Remark 3. Corollary 2 in the context of the model example claims that the Fréchet gradient $\mathscr{K}'(\sigma,U) \in \mathbf{ba}(Q) \times \mathbb{R}^m$ is

$$\mathscr{K}'(\sigma,U) = \Big(\mathscr{K}'_\sigma(\sigma,U), \mathscr{K}'_U(\sigma,U)\Big) =$$
$$\left(-\sum_{j=1}^m \nabla u_j \cdot \nabla \psi_j, \Big(\sum_{j=1}^m \sum_{l=1}^m 2\Big[\int_{E_l} \frac{U_l^j - u_j}{Z_l} ds - I_l^j\Big] \int_{E_l} \frac{\delta_{l,\theta_{kj}} - w^{\theta_{kj}}(s)}{Z_l} ds + 2\beta(U_k - U_k^*)\Big)_{k=1}^m\right). \quad (6.7)$$

6.2. Numerical results for EIT and inverse EIT problems

To test the effectiveness of the gradient descent method, we simulate a realistic model example of the inverse EIT problem which adequately represent the diagnosis of the breast cancer in reality. Simulation and computational analysis consist of three stages as it is outlined in Section 4.2.

Stage 1. By selecting boundary current pattern $I = (I_l)_{l=1}^{16}$ (see Table 1) we simulate the EIT model example with $\sigma = \sigma_{true}$ by solving Problem $\mathscr{I}$ with the gradient descent method described in Section 4.1 (see Remark 2), and identify an optimal control U_{true}. Practical analogy of this step is the implementation of the "current–to–voltage" procedure: by injecting current pattern $I = (I_l)_{l=1}^{16}$ on the electrodes E_l, $l = 1,\ldots,16$, take the measurement of the voltages $U^* = (U_1^*,\ldots,U_{16}^*)$. In our numerical simulations U_{true} is identified with U^*.

The numerical results of *Stage 1* is demonstrated in a Figure 2. Electrical currents $(I_l)_{l=1}^{16}$ specified in Table 1 are injected through 16 electrodes E_l, $l = 1,\ldots,16$, and electrical conductivity field $\sigma(x)$ is assumed to be known, i.e., $\sigma(x) = \sigma_{true}(x)$. Recall that the Problem $\mathscr{I}$ is a convex minimization problem with unique global minimizer $\hat{U}$ and with infima $\mathscr{I}_* = \mathscr{I}(\hat{U}) = 0$ (see Remark 1, Section 4). Figure 2(a) shows the optimal solution for control U (empty blue circles) reconstructed from the initial guess $U_{l,ini}$ (filled black circles) provided in Table 1. Figure 2(b) demonstrates fast convergence with respect to functional in 6 iterations.

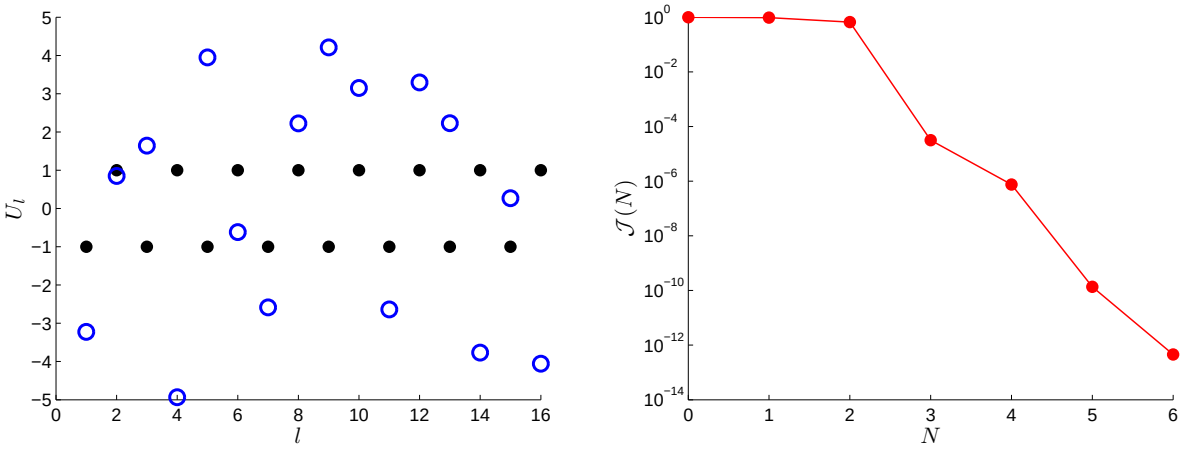

(a) (b)

Figure 2. (a) Empty blue circles show optimal solution $\hat{U}$ reconstructed from the initial guess $U_{l,ini}$ (filled black circles) provided in Table 1. (b) Cost functional $\mathscr{I}(N)$ as a function of optimization iteration N in solving the EIT Problem to find optimal solution $(\hat{u}(x),\hat{U})$.

Stage 2. Solve the Problem $\mathscr{J}$ with limited data $I = (I_l)_{l=1}^{16}$ by the gradient descent method described in Section 4.1, and recover optimal control $(\sigma_{true}, U_{true})$.

Numerical result of *Stage 2* without regularization ($\beta = 0$) is demonstrated in a Figure 3. Furthermore, in all subsequent Figures, we mark the location of four cancer-affected regions from known σ_{true} by dashed circles. Figure 3(b) demonstrates that the electrical conductivity field $\sigma(x)$ is poorly reconstructed without any signature to identify spots with cancer-affected tissues. Fast convergence with respect to functional in just 6 iterations is demonstrated in Figure 7(a). However, there is no convergence with respect to all control parameters as shown in Figure 3(a,b). Although the U-component deviates slightly from actual experimental data U^* (see *Stage 1*) identified with filled red circles in Figure 3(a), the optimal solution $\hat{\sigma}(x)$ obtained for the σ-component is significantly different from the true solution σ_{true}. This is a consequence of the ill-posedness of the inverse EIT problem due to non-uniqueness of the solution.

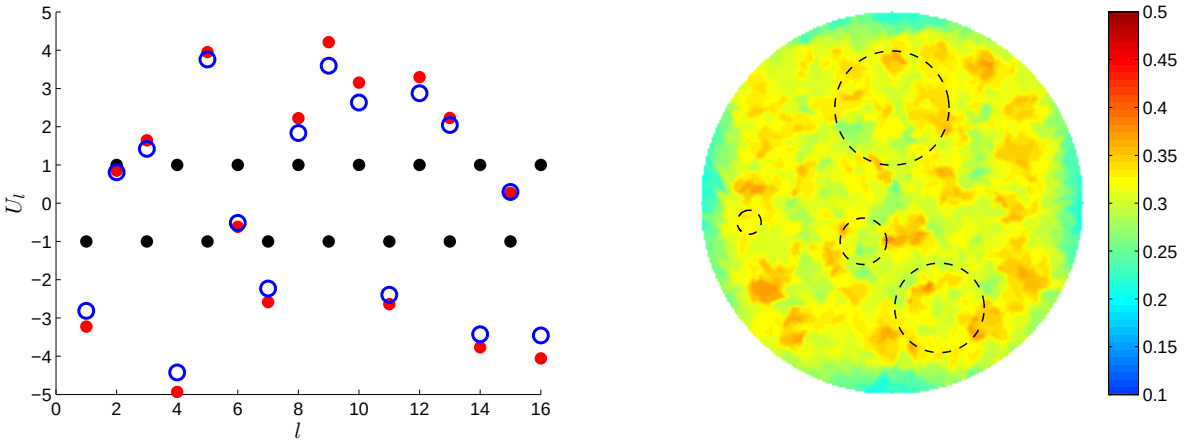

(a) (b)

Figure 3. (a) Empty blue circles show optimal solution $\hat{U}$ reconstructed from the initial guess $U_{l,ini}$ (filled black circles) provided in Table 1. Filled red circles represent actual experimental data U^* (also blue circles in Figure 2(a)). (b) Reconstructed electrical conductivity field $\hat{\sigma}(x)$. Dashed circles represent the location of four cancer-affected regions taken from known σ_{true}.

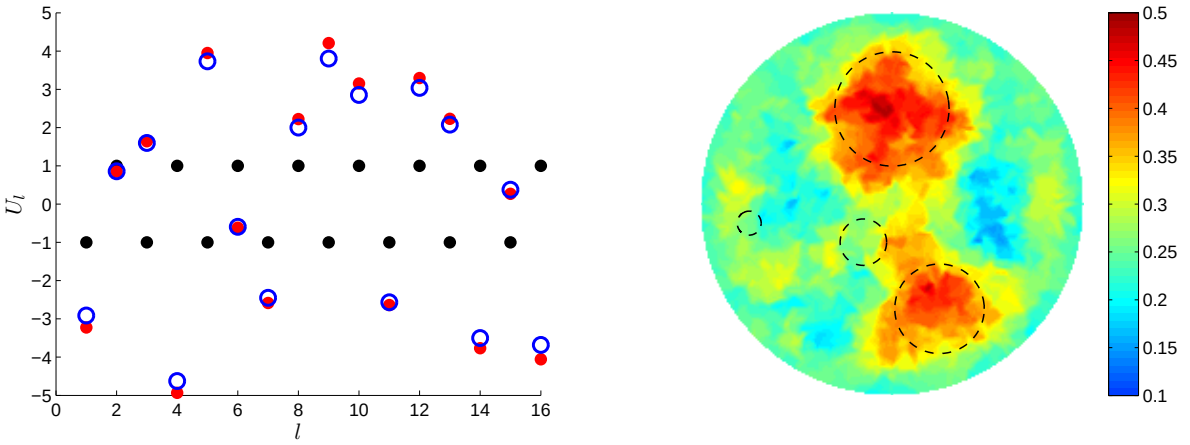

(a) (b)

Figure 4. (a) Empty blue circles show optimal solution $\hat{U}$ reconstructed from the initial guess $U_{l,ini}$ (filled black circles) provided in Table 1. Filled red circles represent actual experimental data U^* (also blue circles in Figure 2(a)). (b) Reconstructed electrical conductivity field $\hat{\sigma}(x)$. Dashed circles represent the location of four cancer-affected regions taken from known σ_{true}.

Stage 3. To increase the size of input data we apply the same set of boundary voltages U_l^* to different electrodes E_l using a "rotation scheme", i.e., we denote $U^1 = U^*, I^1 = I$ and consider 15 new permutations of boundary voltages as in (3.4) applied to electrodes E_1, $E_2, \ldots, E_{16}$ respectively. For each boundary voltage vector U^j we solve elliptic PDE problem (6.1)–(6.3) to obtain the distribution

of electrical potential $u_j(\cdot) = u(\cdot; U^j)$ over boundary ∂Q. By using "voltage–to–current" formula (6.4), we calculate current pattern I^j associated with U^j. Thus, a new set $(I^j)_{j=1}^{16}$ contains 256 input data. Practical analogy of this step is implementation of the "voltage–to–current" procedure: by injecting 15 new sets of voltages $U^j, j = 2, ..., 16$, from (3.4) on the electrodes E_l, $l = 1, \ldots, 16$, take the measurement of the currents $I^j = (I_1^j, \ldots, I_{16}^j)$. Then we solve Problem $\mathscr{K}$ with extended data set by the gradient descent method described in Section 4.1, and recover an optimal control $(\sigma_{true}, U_{true})$.

Numerical result of *Stage 3* without regularization ($\beta = 0$) is demonstrated in a Figure 4. Contrary to previous results, the electrical conductivity field $\sigma(x)$ is reconstructed much better matching the two biggest spots while not perfectly capturing their shapes. Reconstruction result for boundary voltage U is also improved.

Finally, we evaluate the effect of adding regularization term ($\beta > 0$) in the cost functional (3.5). The outcomes with respect to different values of regularization parameter β (blue dots) are shown in Figure 5(a). The dashed line represents the result of optimization with $\beta = 0$. Numerical results demonstrate that small values of β (roughly when $\beta < 10^{-4}$) have no significant effect towards decreasing the values of the cost functional $\mathscr{K}$. Significant improvement at different scales is observed when $\beta > 10^{-1}$. To identify optimal value for β, we examine additionally σ and U solution norms $N_\sigma = \frac{\|\sigma - \sigma_{true}\|_{L_2}}{\|\sigma_{true}\|_{L_2}}$ and $N_U = \frac{|U - U^*|}{|U^*|}$ presented in Figure 5(b). Based on the numerical results, we pick up the value (shown by hexagons) $\beta^* = 0.3162$ as the best value in terms of improvement of solutions simultaneously with respect to both controls σ and U. Figure 6 shows optimal solution $(\hat{\sigma}(x), \hat{U})$ obtained by choosing $\beta^* = 0.3162$. Overall optimization performance in the last case is also enhanced by much faster convergence. Figure 7(b) provides the comparison for convergence results obtained for two different cases, namely without regularization (blue dots), and with regularization with parameter $\beta^* = 0.3162$ (red dots).

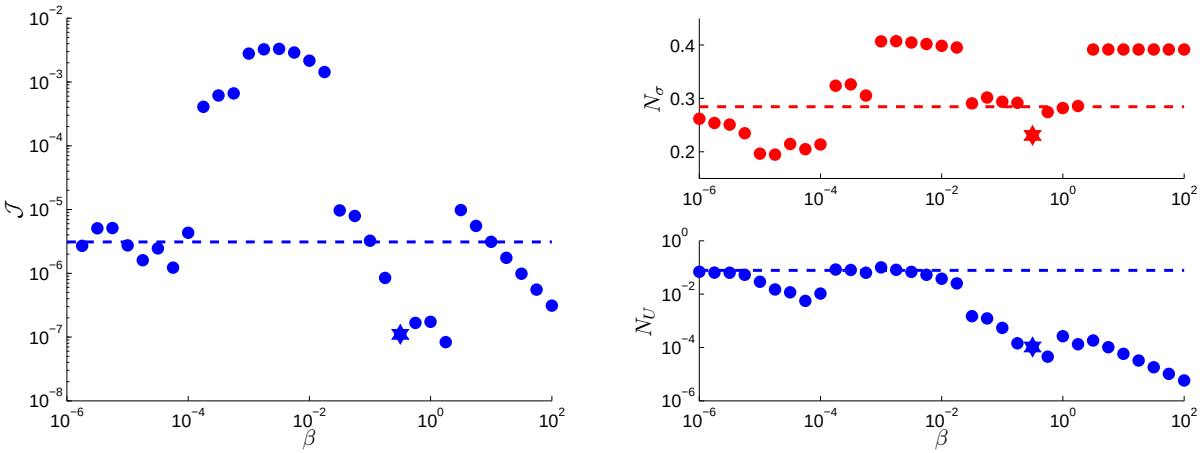

(a) (b)

Figure 5. (a) Cost functional $\mathscr{K}$ values and (b) solution norms $N_\sigma = \frac{\|\sigma - \sigma_{true}\|_{L_2}}{\|\sigma_{true}\|_{L_2}}$ and $N_U = \frac{|U - U^*|}{|U^*|}$ evaluated at termination (dots) for different values of regularization parameter β in (3.1) and (dashed lines) when $\beta = 0$. The best results obtained at $\beta^* = 0.3162$ are shown by hexagons.

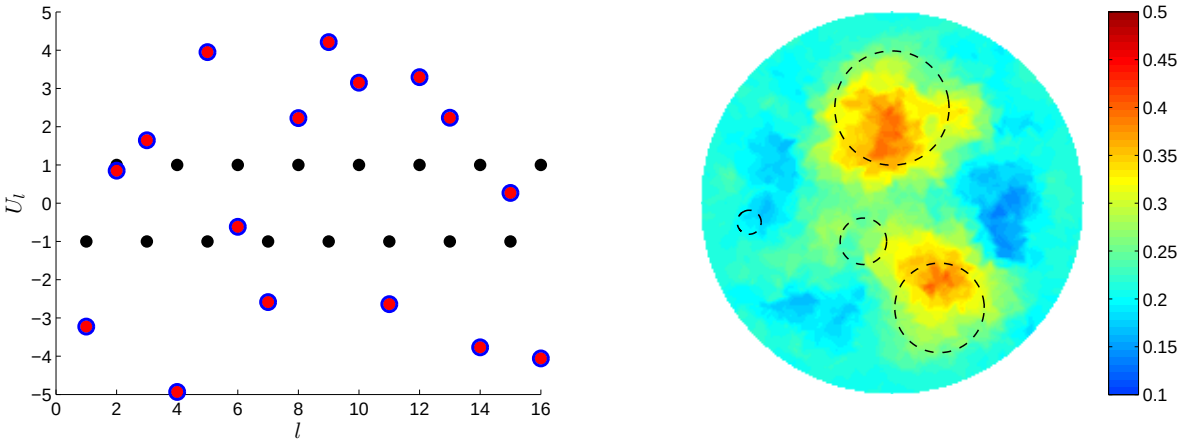

(a) (b)

Figure 6. (a) Empty blue circles show optimal solution $\hat{U}$ reconstructed from the initial guess $U_{l,ini}$ (filled black circles) provided in Table 1. Filled red circles represent actual experimental data U^* (also blue circles in Figure 2(a)). (b) Reconstructed electrical conductivity field $\hat{\sigma}(x)$. Dashed circles represent the location of four cancer-affected regions taken from known σ_{true}. Optimal solution $(\hat{\sigma}(x), \hat{U})$ is obtained by solving the Problem $\mathscr{K}$ with regularization parameter $\beta^* = 0.3162$ in (3.5).

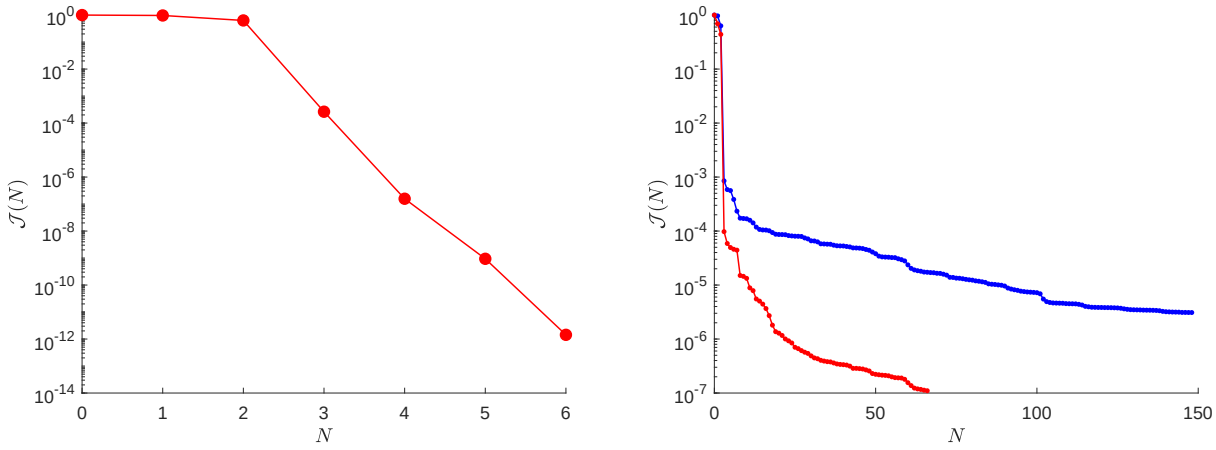

(a) (b)

Figure 7. Cost functional $\mathscr{J}(N)$ as a function of optimization iteration N in solving the EIT Inverse Problem to find optimal solution $(\hat{\sigma}(x), \hat{U})$ (a) without and (b) with applying additional data acquired through rotating boundary voltages U_l. Convergence in (b) is compared for two cases: (blue dots) without regularization, and (red dots) when applying regularization with parameter $\beta^* = 0.3162$.

7. Conclusions

This paper analyzes the inverse EIT problem on recovering electrical conductivity tensor and potential in the body based on the measurement of the boundary voltages on the electrodes for a given electrode current. We analyze the inverse EIT problem in a PDE constrained optimal control framework in the Besov space, where the electrical conductivity tensor and boundary voltages are control parameters, and the cost functional is the norm declinations of the boundary electrode current from the given current pattern and boundary electrode voltages from the measurements. The state vector is a solution of the second-order elliptic PDE in divergence form with bounded measurable coefficients under mixed Neumann/Robin type boundary condition. The following are the main results of the paper:

- The novelty of the control-theoretic model is its adaptation to the clinical situations when additional "voltage-to-current" measurements can increase the size of the input data from the number of boundary electrodes m up to $m!$, while keeping the size of the unknown parameters fixed. Precisely, given m "current-to-voltage" measurements, one can form up to $m!$ permutations of it and generate new "voltage-to-current" measurements. The idea of using permutations of the original voltage measurement implies that the size of the boundary electrode voltage component of the control vector remains unchanged, while up to $m!$ new measurements are gained.
- Existence of the optimal control in the Besov space setting is proved.
- Fréchet differentiability is proved and the formula for the Fréchet gradient expressed in terms of the adjoined problem is derived. A necessary optimality condition is established. An effective numerical method based on the projective gradient method in Besov spaces is developed.
- Numerical analysis of the simulated model example in the 2D case demonstrates that by increasing the number of input boundary electrode currents from m to m^2 through additional "voltage-to-current" measurements the resolution of the electrical conductivity of the body identified via gradient method in Besov space framework is significantly improved.

Conflict of interest

The authors declare there is no conflicts of interest.

References

1. D. S. Holder, *Electrical impedance tomography: methods, history and applications*, CRC Press, 2004.
2. E. Somersalo, M. Cheney, D. Isaacson, Existence and uniqueness for electrode models for electric current computed tomography, *SIAM J. Appl. Math.*, **52** (1992), 1023–1040.
3. S. Laufer, A. Ivorra, V. Reuter, Electrical impedane characterization of normal and cancerous human hepatic tissue, *Physiol. Meas.*, **31** (2010), 995–1009.
4. A. P. Calderon, On an inverse boundary value problem, in Seminar on Numerical Analysis and Its Applications to Continuum Physics, *Soc. Brasileira de Mathematica, Rio de Janeiro*, (1980), 65–73.
5. J. Sylvester, G. Uhlmann, A global uniqueness theorem for an inverse boundary value problem, *Physiol. Meas.*, (1987), 153–169.

6. A. I. Nachman, Reconstructions from boundary measurements, *Ann. Math.*, **128** (1988), 531–576.
7. G. Alessandrini, Stable determination of conductivity by boundary measurements, *Appl. Anal.*, **27** (1988), 153–172.
8. K. Astala, L. Palvarinta, Calderon's inverse conductivity problem in the plane, *Ann. Math.*, **163** (2006), 265–299.
9. C. Kenig, J. Sjöstrand, G. Uhlmann, The Calderon problem with partial data, *Ann. Math.*, **165** (2007), 567–591.
10. C. Kenig, J. Sjöstrand, G. Uhlmann, The Calderon problem with partial data on manifolds and aplications, *Anal. PDE*, **6** (2013), 2003–2048.
11. A. I. Nachman, Global uniqueness for a two-dimensional inverse boundary value problem, *Ann. Math.*, **143** (1996), 71–96.
12. K. Knudsen, M. Lassas, J. Mueller, S. Siltanen, D-Bar method for electrical impedance tomography with discontinuous conductivities, *SIAM J. Appl. Math.*, **67** (2007), 893–913.
13. K. Knudsen, M. Lassas, J. Mueller, S. Siltanen, Reconstructions of piecewise constant conductivities by the D-bar method for electrical impedance tomography, *J. Phys. Conf. Ser.*, **124** (2008), 012029.
14. K. Knudsen, M. Lassas, J. Mueller, S. Siltanen, Regularized D-bar method for the inverse conductivity problem, *Inverse Probl. Imaging*, **3** (2009), 599–624.
15. V. Kolehmainen, M. Lassas, P. Ola, S. Siltanen, Recovering boundary shape and conductivity in electrical impedance tomography, Inverse Problems and Imaging, *Inverse Probl. Imaging*, **7** (2013), 217–242.
16. J. Sylvester, An anisotropic inverse boundary value problem, *Comm. Pure Appl. Math.*, **43** (1990), 201–232.
17. J. M. Lee, G. Uhlmann, Determining anisotropic real-analytic conductivities by boundary measurements, *Comm. Pure Appl. Math.*, **42** (1989), 1097–1112.
18. M. Lassas, G. Uhlmann, On determining a Riemannian manifold from the Dirichlet-to-Neumann map, *Ann. Sci. Ecole Norm. Sup.*, **34** (2001), 771–787.
19. M. Lassas, G. Uhlmann, M. Taylor, The Dirichlet-to-Neumann map for complete Riemannian manifolds with boundary, *Commun. Anal. Geom.*, **11** (2003), 207–221.
20. M. I. Belishev, The Calderon problem for two-dimensional manifolds by the BC-Method, *SIAM J Math. Anal.*, **35** (2003), 172–182.
21. K. Astala, M. Lassas, L. Palvarinta, Calderon's inverse problem for anisotropic conductivity in the plane, *Comm. PDEs*, **30** (2005), 207–224.
22. R. V. Kohn, M. Vogelius, Determining conductivity by boundary measurements, *Comm. Pure Appl. Math.*, **37** (1984), 289–298.
23. R. V. Kohn, M. Vogelius, Determining conductivity by boundary measurements. II. Interior results, *Comm. Pure Appl. Math.*, **38** (1985), 643–667.
24. W. R. B. Lionheart, Conformal uniqueness results in anisotropic electrical impedance imaging, *Inverse Problems*, **13** (1997), 125–134.

25. G. Alessandrini, R. Gaburro, The local Calderon problem and the determination at the boundary of the conductivity, *Comm. PDEs*, **34** (2009), 918–936.
26. R. Gaburro, W. R. B. Lionheart, Recovering Riemannian metrics in monotone families from boundary data, *Inverse Probl.*, **25** (2009), 045004.
27. R. Gaburro, E. Sinicich, Lipschitz stability for the inverse conductivity problem for a conformal class of anisotropic conductivities, *Inverse Probl.*, **31** (2015), 015008.
28. G. Alessandrini, M.V. de Hoop, R. Gaburro, Uniqueness for the electrostatic inverse boundary value problem with piecewise constant anisotropic conductivities, *Inverse Probl.*, **33** (2017), 125013.
29. A. Lechleiter, A. Rieder, Newton regularization for impedance tomography: convergence by local injectivity, *Inverse Probl.*, **24** (2008), 065009.
30. B. Harrach, Uniqueness and Lipschitz stability in electrical impedance tomography with finitely many electrodes, *Inverse Probl.*, **35** (2019), 024005.
31. M. Ammari, H. Kang, Reconstruction of Small Inhomogeneities from Boundary, *Springer*, 2004.
32. O. Kwon, J. K. Seo, J. R. Yoon, A real-time algorithm for the location search of discontinuous conductivities with one measurement, *Inverse Probl.*, **55** (2002), 1–29.
33. H. Ammari, L. Qiu, F. Santosa, W. Zhang, Determining anisotropic conductivity using diffusion tensor imaging data in magneto-acoustic tomography with magnetic induction, *Inverse Probl.*, **33** (2017), 125006.
34. J. K. Seo, E. J. Woo, Magnetic resonance electrical impedance tomography, *SIAM Rev.*, **53** (2011), 40–68.
35. T. Widlak, O. Scherzer, Hybrid tomography for conductivity imaging, *Inverse Probl.*, **28** (2012), 084008.
36. H. Ammari, G. S. Alberti, B. Jin, J. K. Seo, W. Zhang, The linearized inverse problem in multifrequency electrical impedance tomography, *SIAM J. Imaging Sci.*, **9** (2016), 1525–1551.
37. J. K. Seo, J. Lee, S. W. Kim, H. Zribi, E.J. Woo, Frequency-difference electrical impedance tomography: algorithm development and feasibility study, *Phys. Meas.*, **29** (2008), 929–941.
38. B. Jin, Y. Xu, J. Zou, A convergent adaptive finite element method for electrical impedance tomography, *IMA J. Numer. Anal.*, **37** (2017), 1520–1550.
39. G. Matthias, J. Bangti, X. Lu, An analysis of finite element approximation in electrical impedance tomography, *Inverse Probl.*, **30** (2014), 045013.
40. B. Jin, T. Khan, P. Maass, A reconstruction algorithm for electrical impedance tomography based on sparsity regularization, *Int. J. Numer. Methods*, **89** (2012), 337–353.
41. B. Harrah, M. N. Minh, Enhancing residual-based techniques with shape reconstruction features in Electrical Impedance Tomography, *Inverse Probl.*, **32** (2016), 125002.
42. M. Alsaker, J. L. Mueller, A *D*-bar algorithm with a priori information for 2-dimensional electrical impedance tomography, *SIAM J. Imaging Sci.*, **9** (2016), 1619–1654.
43. M. Dodd, J. Mueller, A real-time *D*-bar algorithm for 2d electrical impedance tomography data, *Inverse Probl. Imaging*, **8** (2014), 1013–1031.

44. S. J. Hamilton, M. Lassas, S. Siltanen , A direct reconstruction method for anisotropic electrical impedance tomography, *Inverse Probl.*, **30** (2014), 075007.
45. S. J. Hamilton, M. Lassas, S. Siltanen , A hybrid segmentation and *D*-bar method for electrical impedance tomography, *SIAM J. Imaging Sci.*, **9** (2016), 770–793.
46. N. Hyvönen, L. Pälvärinta, J. P. Tamminen, Enhancing D-bar reconstructions for electrical impedance tomography with conformal maps, *Inverse Probl. Imaging*, **12** (2018), 373–400.
47. M. V. Klibanov, J. Li, W. Zhang , Convexification of electrical impedance tomography with restricted Dirichlet-to-Neumann map data, *Inverse Probl.*, **35** (2019), 035005.
48. J. P. Kaipio, E. Somersalo , *Statistical and Computational Inverse Problems*, Springer, 2005.
49. J. P. Kaipio, V. Kolehmainen, E. Somersalo, M. Vauhkonen, Statistical inversion and Monte Carlo sampling methods in electrical impedance tomography, *Inverse Probl.*, **16** (2000), 1487.
50. J. P. Kaipio, V. Kolehmainen, M. Vauhkonen, E. Somersalo, Inverse problems with structural prior information, *Inverse Probl.*, **15** (1999), 713.
51. S. Lasanen, J. M. L. Huttunen, L. Roininen, Whittle-Matern priors for Bayesian statistical inversion with applications in electrical impedance tomography, *Inverse Probl. Imaging*,(2014), 561–586.
52. M. Lassas, E. Saksman, S. Siltanen, Discretization-invariant Bayesian inversion and Besov space priors, *Inverse Probl. Imaging*, (2009), 87–122.
53. M. Dunlop, A. M. Stuart, The Bayesian formulation of EIT: analysis and algorithms, *Inverse Probl. Imaging*, **10** (2016), 1007–1036.
54. L. C. Evans, Partial Differential Equations, *Graduate studies in mathematics*, 1998.
55. U. G. Abdulla, On the Optimal Control of the Free Boundary Problems for the Second Order Parabolic Equations. I. Well-posedness and Convergence of the Method of Lines, *Inverse Probl. Imaging*, **7** (2013), 307–340.
56. U. G. Abdulla, On the Optimal Control of the Free Boundary Problems for the Second Order Parabolic Equations. II. Convergence of the Method of Finite Differences, *Inverse Probl. Imaging*, **10** (2016), 869–898.
57. U. G. Abdulla, J. M. Goldfarb, Fréchet differentiability in Besov spaces in the optimal control of parabolic free boundary problems, *J. Inverse Ill Posed Probl.*, **26** (2018), 211–227.
58. U. G. Abdulla, E. Cosgrove, J. Goldfarb, On the Fréchet differentiability in optimal control of coefficients in parabolic free boundary problems, *Evol. Equ. Control. Theory*, **6** (2017), 319–344.
59. U. G. Abdulla, B. Poggi, Optimal control of the multiphase Stefan problem, *Appl. Math. Optim.*, **80** (2019), 479–513.
60. U. G. Abdulla, V. Bukshtynov, A. Hagverdiyev, Gradient method in Hilbert-Besov spaces for the optimal control of parabolic free boundary problems, *J. Comput. Appl. Math.*, **346** (2019), 84–109.
61. U. G. Abdulla, B. Poggi, Optimal Stefan problem, *Calc. Var. Partial Differ. Equ.*, **59** (2020), 1–40.
62. O. V. Besov, V. P. Il'in, S. M. Nikol'skii, Integral Representations of Functions and Imbedding Theorems, Volume I, Winston & Sons, Washington, D.C.; Halsted Press [John Wiley & Sons], New York -Toronto, Ont.-London, 1978, viii+345 pp.

63. O. V. Besov, V.P. Il'in, S.M. Nikol'skii, Integral Representations of Functions and Imbedding Theorems, Volume II, Winston & Sons, Washington, D.C.; Halsted Press [John Wiley & Sons], New York -Toronto, Ont.-London, 1979, vii+311 pp.
64. S. M. Nikol'skii, Approximation of Functions of Several Variables and Imbedding Theorems, Springer-Verlag, New York-Heidelberg, 1975, vii+418 pp.
65. P. E. Gill, W. Murray, M.A. Saunders, SNOPT: An SQP algorithm for large-scale constrained optimization, *SIAM Rev.*, **47** (2005), 99–131.
66. F. Hecht, New development in FreeFem++, *J. Numer. Math.*, **20** (2012), 251–265.